Available online at www.sciencedirect.com

ScienceDirect

Applied Surface Science 253 (2007) 8782–8787

applied surface science

www.elsevier.com/locate/apsusc

Influence of deposition conditions on the microstructure of oxides thin films

Guanglei Tian [a,c,*], Shigang Wu [b,c], Kangying Shu [a], Laishun Qin [a], Jianda Shao [c]

[a] College of Science, China Jiliang University, Hangzhou 310018, PR China

[b] School of Material Science and Engineering, Shandong University of Technology, Zibo 255049, PR China

[c] Shanghai Institute of Optics and Fine Mechanics, Chinese Academy of Sciences, Shanghai 201800, PR China

Received 28 September 2006; received in revised form 25 April 2007; accepted 25 April 2007

Available online 5 May 2007

Abstract

Thin films of ZrO_2, HfO_2 and TiO_2 were deposited on kinds of substrates by electron beam evaporation (EB), ion assisted deposition (IAD) and dual ion beam sputtering (DIBS). Then some of them were annealed at different temperatures. X-ray diffraction (XRD) was applied to determine the crystalline phase and the grain size of these films, and the results revealed that their microstructures strongly depended on the deposition conditions such as substrate, deposition temperature, deposition method and annealing temperature. Theory of crystal growth and migratory diffusion were applied to explain the difference of crystalline structures between these thin films deposited and treated under various conditions.

Keywords: X-ray diffraction; Crystal structure; Nucleation; Oxides films

1. Introduction

As critical component of less than 2 nm for semiconductor devices, in the past several decades, a large number of alternative dielectric materials, including metal oxides such as HfO_2, TiO_2, Ta_2O_5, ZrO_2 and Al_2O_3 [1–4], had been studied to achieve higher speed, density and computational ability. At the same time, due to their strong resistance to laser-induced damage and rather wide transparent region of spectrum, they are also used as high index refractive materials for optical coatings stacks. It was well known that many different procedures for the preparation of TiO_2 films were reported [5,6], and with all these deposition methods, these films could be made with largely varying structural and optical properties [7,8]. Their properties and structure are known to be easily affected by the deposition conditions such as the substrate temperature and oxygen partial pressure as well as the post-deposition heat-treatment. Crystal structure of ZrO_2, HfO_2 and TiO_2 has great effect on their physical properties, and a large variety of papers have been devoted to this field [9–12]. As for TiO_2 thin film, when it is rutile and the grain size decrease from 63 nm in diameter to amorphism, the laser-induced damage threshold (LIDT) of TiO_2 film monotonously increases from 1 to 9 J/cm^2 [13,14]. ZrO_2 films containing monoclinic phases had higher damage threshold than others, and annealing at high temperature facilitates the formation of monoclinic phase of zirconia [15].

In this article, ZrO_2, HfO_2 and TiO_2 thin films were prepared with different deposition methods and under the different deposition conditions such as substrate, deposition temperature and annealing temperature, and influence of technological conditions of the deposition process on the microstructure of thin films were investigated.

2. Experiments

2.1. Sample preparation methods

In the experiments, the substrates of polished fused silica, K9, $LiNbO_3$ and YAG were used. All these substrates come from SINCERA, a company providing optical component and service. These substrates experience fine polishing before deposition, and the surface degree of finish belongs to the

* Corresponding author at: College of Science, China Jiliang University, Hangzhou 310018, PR China. Tel.: +86 571 86835738.

E-mail address: gltian@siom.ac.cn (G. Tian).

0169-4332/$ – see front matter
doi:10.1016/j.apsusc.2007.04.073

second level. The surface optical quality is 40–20 (Scratch/dot), and the surface shape is 0.5λ (λ = 632.8 nm). Firstly, these substrates were immersed to acetone for several hours to get rid of oil pollution on the surface, and then cleaned with petroleum ether at 253 K in ultrasound cleaner for 50 s twice.

ZrO_2 films were deposited by electron beam evaporation. The ZrO_2 tablets with the purity of 99.99%, provided by General Research Institute for Nonferrous Metals (GRINM), were used as starting material, the deposition temperature is 573 K and the ambient oxygen pressure is 7.3×10^{-3} Pa. ZrO_2 thin films with optical thickness of 2λ/4 (λ = 500 nm) were prepared on the fused silica and YAG under optical control.

TiO_2 thin films were deposited on the $LiNbO_3$ and fused silica at 573 K by electron beam evaporation. The starting materials (provided by GRINM) were TiO crushed aggregates with the purity of 99.99%. Before deposition, the chamber was cryogenically pumped to a base pressure of 7.3×10^{-3} Pa and oxygen was introduced to keep oxygen partial pressure of 2.6×10^{-2} Pa. The films with optical thickness of 8λ/4 (λ = 500 nm) were prepared under optical control.

HfO_2 films were deposited on K9 glass with electron beam evaporation, ion assisted deposition (IAD) and dual ion beam sputtering (DIBS), respectively. The deposition temperature of films by EB and IAD is 573 K, and that by DIBS is 383 K. The starting materials (provided by GRINM) by EB are HfO_2 tablets with the purity of 99.99%. However, the HfO_2 films by IAD and DIBS were prepared with metal hafnium, and the purity of metal Hf is 99.9%.

2.2. Determination of structure

Crystalline phase of the films was identified by X-ray diffraction which was Rigaku D/max-3C diffractometer with Cu Kα, λ = 1.5406 Å. The XRD method was used to study the change of ZrO_2, TiO_2 and HfO_2 structure and grain size caused by post-deposition annealing. The step width is 0.02°. The grain size can be calculated by Scherrer's equation:

$$C = \frac{0.89\lambda}{B\cos\theta} \quad (1)$$

where C is the grain size, λ the wavelength of X-ray, B the full width at half-maximum of diffraction peak (FWHM), and θ is the diffraction angle. In this article, the average error of grain size by the diffractometer is about 1 nm.

3. Results

3.1. XRD results of ZrO_2 films on different substrates

The XRD patterns (Fig. 1) show that the ZrO_2 thin films on different substrates exhibit tetragonal phase before annealing [15]. When annealed at 673 K, the peaks of tetragonal phase become more acute, and it was attributed to grain growth after annealing. When the coatings were annealed at 1073 K, compared with annealed at low temperature, the diffraction intensity of tetragonal phase decreased, and at the same time there was appearance of monoclinic phase in coatings. We can assume that part of tetragonal phase of ZrO_2 coatings transformed into monoclinic phase with the increasing of annealing temperature, and here the coatings exhibited two phases coexisting.

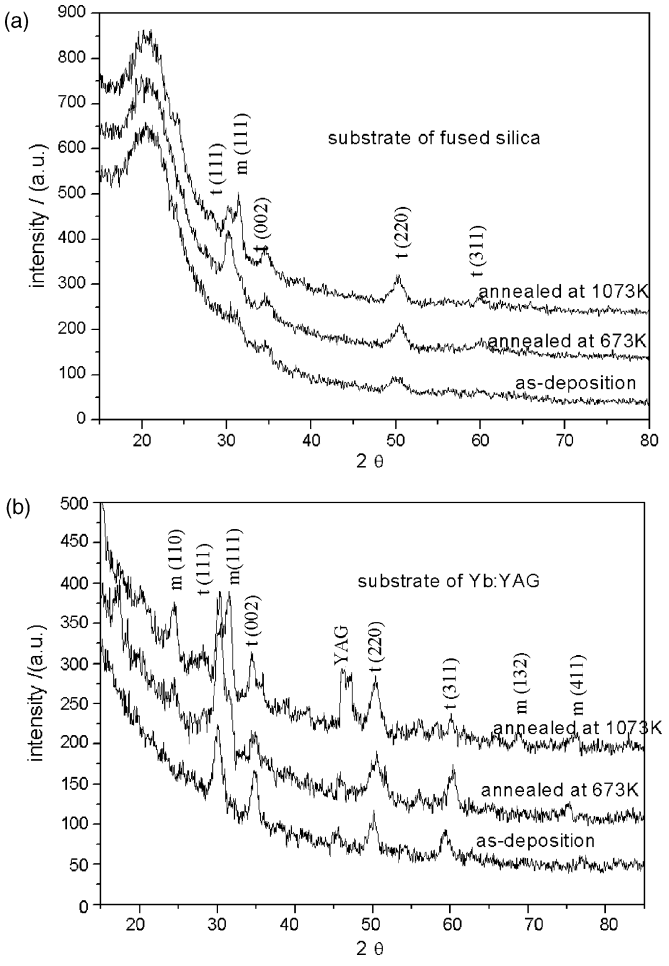

Fig. 1. X-ray diffraction patterns of ZrO_2 coatings on deferent substrates: (a) ZrO_2 thin films on fused silica and (b) ZrO_2 thin films on YAG.

As for crystalline structure of ZrO_2 coatings, there is evident difference between on YAG and on fused silica. Before annealing, the characteristic peak of only crystal plane (1 1 1), (0 0 2), (2 2 0) of t-ZrO_2 on fused silica, which simultaneously is rather weak, appear, whereas on YAG substrate characteristic peak of t-ZrO_2 thin films crystal plane (1 1 1), (0 0 2), (2 2 0) and (3 3 1) come into being, and intensity of these peaks on YAG is much stronger than that on fused silica. Here we can draw following conclusion that when deposited at 573 K, tetragonal phase of ZrO_2 coatings on YAG formed more easily than they do on fused silica. When the annealing temperature reached 1073 K, on substrate of YAG characteristic peaks of m-ZrO_2 coatings crystal plane (1 1 0), (1 1 1) appear, and at the same time the intensity of these peaks is rather strong. However, only diffraction peak of crystal plane (1 1 1) of m-ZrO_2 coatings on fused silica appeared (Table 1).

Table 1
Grain size of ZrO_2 coatings annealed for various temperatures

Group	t(1 1 1)		t(2 2 0)	
	B (°)	*C* (nm)	*B* (°)	*C* (nm)
Fused silica				
As-deposition	–	–	1.825	6.8
Annealed at 673 K	1.350	6.7	1.140	10.9
Annealed at 1073 K	1.050	9.1	1.080	11.4
YAG				
As-deposition	1.140	8.0	0.900	13.7
Annealed at 673 K	1.110	8.2	0.720	17.2
Annealed at 1073 K	1.080	8.4	0.850	13.4

Table 2
Evolution of FWHM and grain size at An (1 0 1) and An (0 0 4) peak of TiO_2 coatings annealed at different temperatures

Annealing temperature (K)	An(1 0 1)		An(0 0 4)	
	B (°)	*C* (nm)	*B* (°)	*C* (nm)
As-deposition	–	–	–	–
573	0.379	23.0	0.397	25.1
773	0.237	36.7	0.314	31.7
973	0.179	48.6	0.236	42.2
1173	0.151	57.6	0.292	34.1
1373	0.147	59.2	0.225	44.2

3.2. XRD results of TiO_2 films on different substrates

3.2.1. Crystalline structure of TiO_2 thin films on fused silica

Fig. 2 illustrates the XRD patterns of TiO_2 thin films as-deposited and annealed at different temperatures [16]. It is found that the TiO_2 coatings exhibit amorphous structure before annealing, and regardless of annealing temperature, there is only anatase structure TiO_2 in annealed coatings. From diffraction patterns, we can see that annealed TiO_2 coatings exhibit characteristic peaks of anatase crystal plane (1 0 1), (0 0 4) and (1 0 5), and with the annealing temperature increasing, the half-maximum of diffraction peak (FWHM) gradually decrease in terms of crystal plane (1 0 1). When the annealing temperature reaches 1373 K, other characteristic peaks of anatase crystal plane (1 0 3), (2 0 0) and (2 0 4) come in to being, but the intensity of these peaks is very weak (Table 2).

3.2.2. Crystalline structure of TiO_2 thin films on $LiNbO_3$

In order to investigate the influence of different substrates on the TiO_2 films structure, TiO_2 films were deposited on the $LiNbO_3$ substrates, and some of them were annealed at different temperatures. The XRD patterns are shown in Fig. 3, and the strong peaks belong to the diffraction peaks of the substrates of crystal $LiNbO_3$ rather than TiO_2 films. The results reveal that

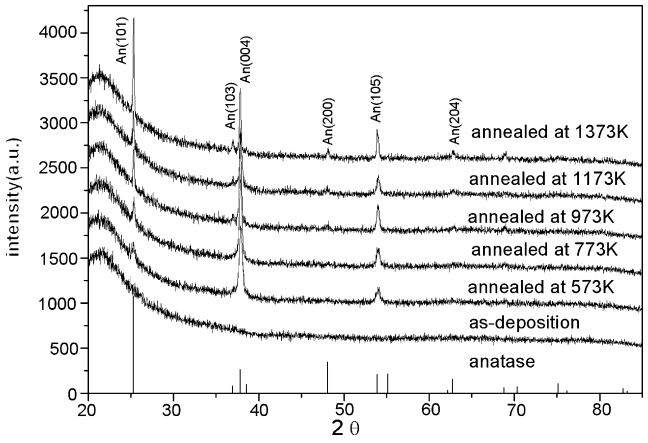

Fig. 2. X-ray diffraction patterns of TiO_2 thin films annealed at different temperatures.

though being prepared on the $LiNbO_3$ substrates, TiO_2 films is also amorphous, and the crystalline phase of TiO_2 films annealed at different temperatures on $LiNbO_3$ is the same as that of films on the fused silica, which indicates that the $LiNbO_3$ substrates has little effects on the crystalline phase of TiO_2 films and is different from the dependence of ZrO_2 films structure on the substrates.

3.3. XRD results of HfO_2 films prepared by different deposition technique

3.3.1. Crystalline structure of HfO_2 thin film by EB at different deposition temperatures

Fig. 4 shows that when HfO_2 thin films were deposited at low temperatures, they exhibit amorphous structure, and when the deposition temperature reaches 723 K, the films structure also transforms to polycrystalline states from amorphous states, which indicates that the crystalline structure and grain size strongly depend on the deposition temperature, and high deposition temperature can facilitate nucleation and crystallization. So we can assume that if the deposition temperature is satisfactory in the preparation process, the films always can exhibit polycrystalline states.

3.3.2. Crystalline structure comparison of HfO_2 thin film by IAD, EB and DIBS

The XRD diffraction patterns of HfO_2 thin films by IAD, EB and DIBS are shown in Figs. 5 and 6, and here the deposition temperature of films deposited by EB and IAD is 573 K, and that of films by DIBS is 383 K. Though deposition temperature of the films by both EB and IAD is 573 K, the HfO_2 films by EB are amorphous and the films by IAD exhibit polycrystalline states. As for the films by DIBS, its deposition temperature is nothing more than 383 K, but they still exhibit polycrystalline states. Comparing Fig. 5 with Fig. 6, we can see that there is a great difference between IAD and DIBS in diffraction patterns.

4. Discussion

When thin films were deposited on the different substrates, whether films can be deposited with polycrystalline or amorphous states depends on the migratory diffusion ability and the nucleation work for critical crystal nucleus on the substrates.

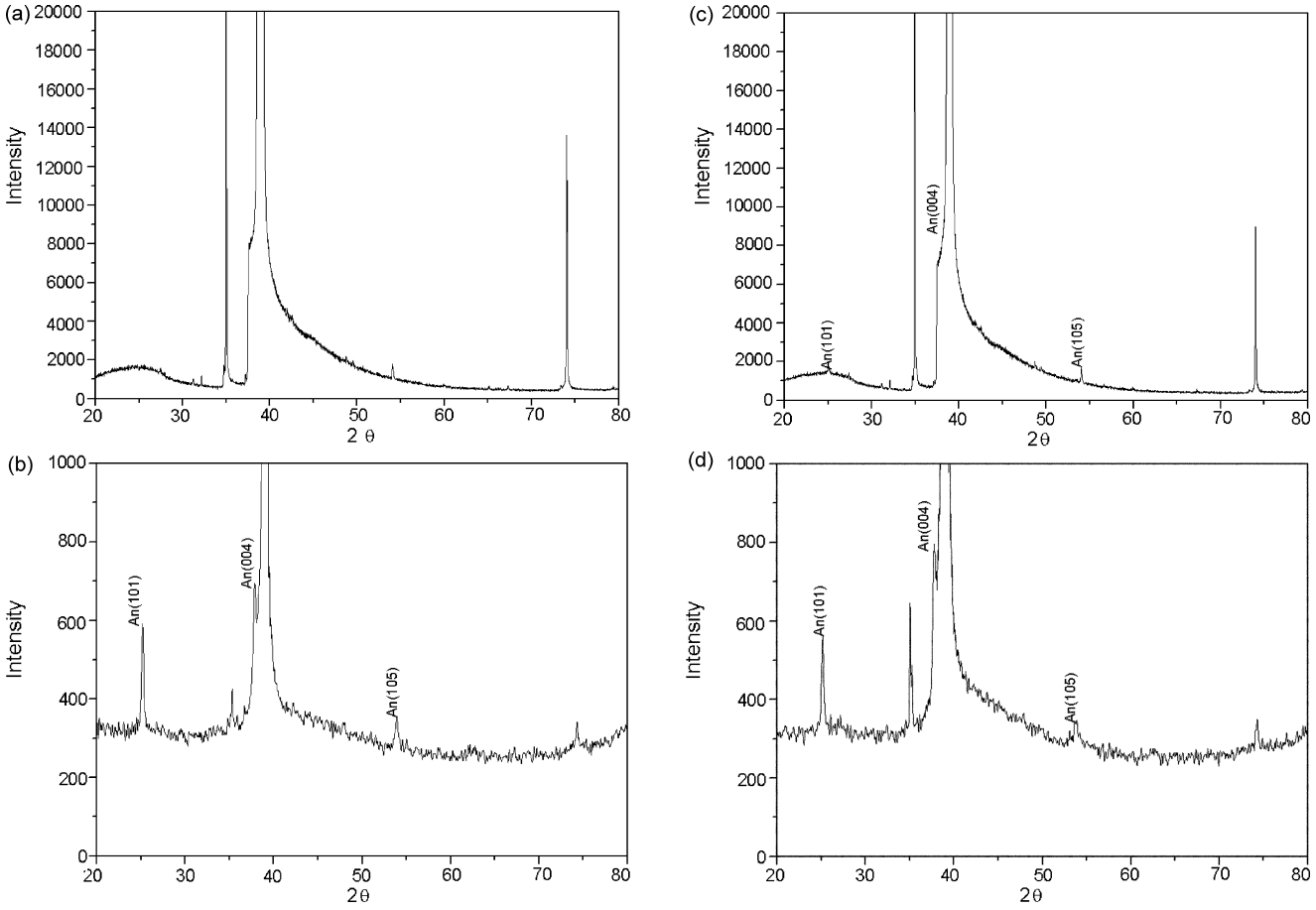

Fig. 3. X-ray diffraction patterns of TiO_2 thin films annealed at different temperatures on $LiNbO_3$ substrates: (a) as-deposition; (b) annealed at 573 K; (c) annealed at 773 K; (d) annealed at 973 K.

When the metal oxide films were deposited on the substrate, the diffusion coefficient can be written as [17]:

$$D = D_0 \exp\left(-\frac{E}{\kappa T}\right) \tag{2}$$

where D is the self-diffusion coefficient, E the diffusion activation energy, and T is the deposition temperature. From the equation above, we can see that with the substrate temperature increasing, the self-diffusion coefficient also increases.

When the atoms cluster to nucleation on the surface of substrate, which is in most cases of films growth and belongs to heterogeneous nucleation, then the variation of the Gibbs free energy for crystallite system can be expressed as [18]:

$$\Delta G(r) = \left[-\frac{4/3\pi r^3}{\Omega_s}\Delta g + 4\pi r^2 \sigma_{SL}\right] f(\theta) \tag{3}$$

where $\Delta G(r)$ is the variation of the Gibbs free energy for the transformation from amorphous phase into a crystallite ($\Delta G < 0$), r the radius of the crystallite, Ω_s the volume of an atom, Δg the reduced Gibbs free energy for the transformation from an atom amorphous phase into crystallite, and σ_{SL} is the surface tension of amorphous and crystallite interface. Where $f(\theta)$ is the function of substrate surface tension. Critical radius of crystal nucleus can be presented as [18]:

$$r_C = \frac{2\sigma_{LS}\Omega_s}{\Delta g} \tag{4}$$

Crystal nucleus can further grow into crystallites and polycrystalline films on the condition that the radius of crystal

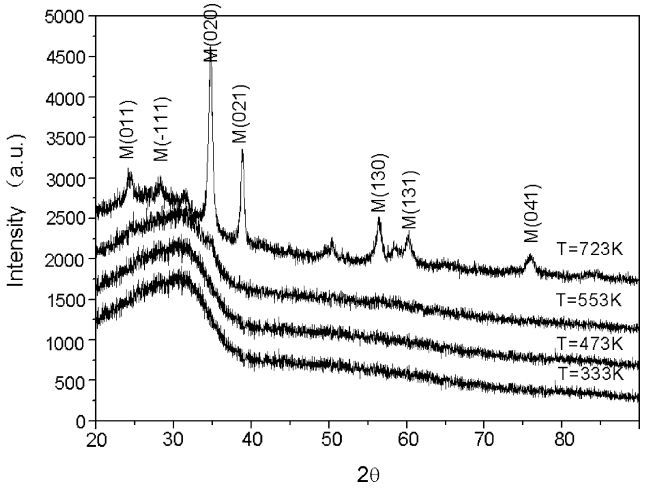

Fig. 4. X-ray diffraction patterns of HfO_2 coatings deposited at different temperatures.

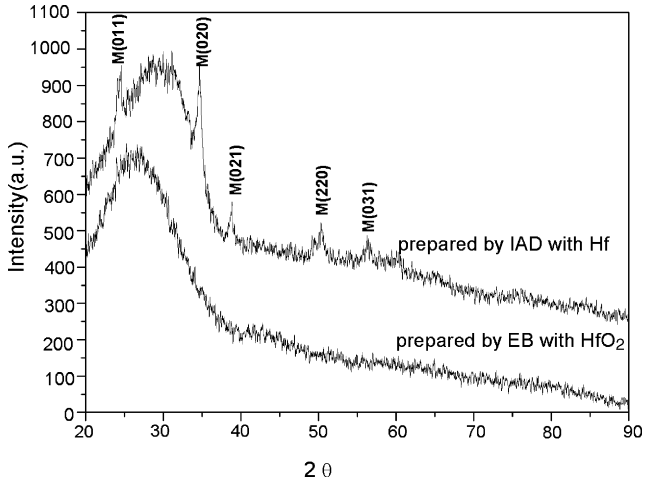

Fig. 5. X-ray diffraction patterns of HfO_2 coatings prepared by IAD and EB.

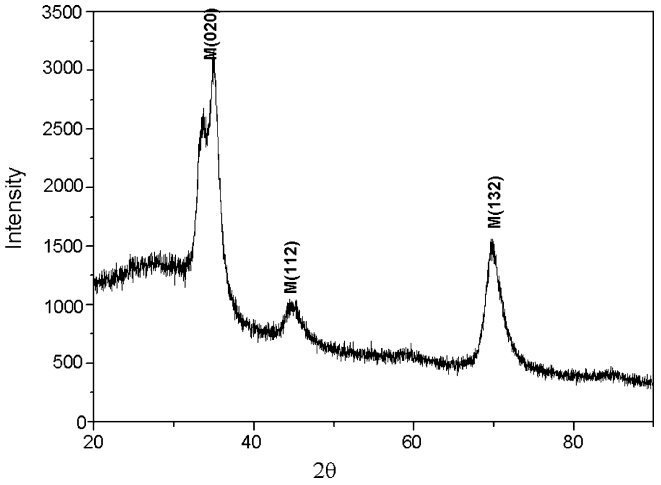

Fig. 6. X-ray diffraction patterns of HfO_2 coatings prepared by DIBS.

nucleus is greater than this critical value, and then the nucleation work for critical crystal nucleus can be written as

$$\Delta G_C(r_C) = \frac{16\pi\Omega_s^2\sigma_{LS}^3}{3\Delta g^2} f(\theta) \quad (5)$$

The relationships (2) and (5) indicate that whether films can nucleate to grow into polycrystalline and even single crystal states not only depends on the properties of thin films material but also is determined by the properties of the substrate surface.

Though being prepared on fused silica substrate at the same deposition temperature, ZrO_2 film is polycrystalline but TiO_2 film is amorphous, which mainly results from the following two reasons: firstly, for TiO_2 thin films, the deposition temperature of 573 K is low, so the kinetic energy of TiO_2 molecules is deficient in getting over potential barrier when molecules migrate on the substrate; secondly, in terms of Eq. (3), TiO_2 films system cannot overcome the barrier at the initial stages of nucleation.

As far as ZrO_2 thin films are concerned, their diffusion and nucleation on substrate of YAG are easier than on fused silica at the initial stages of films deposition. When we stop the deposition process, the grain size of ZrO_2 films on YAG substrate is larger than that on fused silica, so XRD diffraction peak of ZrO_2 films on YAG is much stronger than fused silica, which is consistent with Fig. 1 and Table 1.

When HfO_2 films were prepared at rather low temperatures, the migration ability of films molecule on the substrates is very poor, so HfO_2 film is amorphous. With the deposition temperature increasing, the migration ability of molecule also increases and at the same time, the nucleation work for critical crystal nucleus decreases. So, our experimental results (Fig. 4) indicate that HfO_2 films exhibit polycrystalline at temperature 723 K but exhibit amorphous state below this temperature.

As far as HfO_2 films prepared by different methods are concerned, it is difficult to completely explain the great difference of film structure between the different methods. The most difference between these methods lies in the kinetic energy of molecule reaching substrates, and the kinetic energy of molecule reaching substrates by electron beam evaporation, IAD and DIBS is about 0.3, 5 and 30–50 eV, respectively [19]. The films molecule bumping on the substrates can be regarded as nonelastic collision process, and it may be the kinetic energy of film molecule that plays an important role in the great difference of film structure. Most of the kinetic energy of films molecule is transformed into heat energy, so the deposition temperature is low with IAD and DIBS methods, but the actual temperature substrates is likely to be higher than the deposition temperature. So HfO_2 films prepared by IAD and DIBS, in comparison with films by EB, exhibits polycrystalline states (Figs. 5 and 6) with rather low deposition temperature, and there is a great difference between the film structures by IAD and DIBS.

5. Conclusions

As far as ZrO_2 films are concerned, they are prepared on the substrates of both YAG and fused silica at the same temperature, and the films on YAG substrates crystallize much earlier than on the fused silica. With the annealing temperature increasing, the crystallinity of ZrO_2 films is also increases. However, TiO_2 films prepared on the substrates of $LiNbO_3$ and fused silica exhibit amorphous at the same temperature. For HfO_2 films, high deposition temperatures help films to crystallize and decrease the nucleation work for critical crystal nucleus. Though the deposition temperature of HfO_2 films prepared by IAD and DIBS is lower than that of films by EB, the HfO_2 films by IAD and DIBS exhibit polycrystalline and films by EB is amorphous. The film crystallization can be regarded as a process of crystal growth, and whether the films can crystallize depends on the migratory diffusion ability of molecule and the nucleation work for critical crystal nucleus.

References

[1] T. Mori, M. Fujiwara, R.R. Manory, I. Shimizu, T. Tanaka, Surf. Coat. Technol. 169–170 (2003) 528–531.
[2] B.-Y. Tsuia, H.-W. Chang, J. Appl. Phys. 93 (2003) 10119–10124.
[3] V. Mikhelashvili, G. Eisenstein, J. Appl. Phys. 89 (2001) 3256–3269.

[4] B.R. Weinberger, R.B. Garber, Appl. Phys. Lett. 66 (18) (1995) 2409–2411.
[5] G.K.L. Goh, C.P.K. Liew, J. Kim, T.J. White, J. Cryst. Growth 291 (2006) 94–99.
[6] K. Yokota, Y. Yano, K. Nakamura, M. Ohnishi, F. Miyashita, Nucl. Instrum. Meth. Phys. Res. Sect. B 242 (2006) 393–395.
[7] K. Narashimha Rao, S. Mohan, J. Vac. Sci. Technol. A 8 (4) (1990) 3260–3264.
[8] C.-C. Ting, S.-Y. Chen, D.-M. Liu, J. Appl. Phys. 88 (2000) 4628–4633.
[9] J.S. Kim, H.A. Marzouk, P.J. Reucroft, Thin Solid Film 254 (1–2) (1995) 33–38.
[10] B. Andre, L. Poupinet, G. Ravel, J. Vac. Sci. Technol. A 18 (5) (2000) 2372–2377.
[11] T. Asanuma, T. Matsutani, T. Mihara, M. Kiuchi, J. Appl. Phys. 95 (2004) 6011–6016.
[12] L. Pereira, P. Barquinha, E. Fortunato, R. Martins, Mater. Sci. Eng. B 118 (2005) 210–213.
[13] W.H. Lowdermilk, D. Milam, F. Rainer, Thin Solid Films 73 (1980) 155–166.
[14] Y. Zhao, Y. Wang, H. Gong, J. Shao, Z. Fan, Appl. Surf. Sci. 210 (2003) 353–358.
[15] G. Tian, J. Huang, T. Wang, H. He, J. Shao, Appl. Surf. Sci. 239 (2005) 201–208.
[16] G. Tian, L. Dong, C. Wei, J. Huang, H. He, J. Shao, Opt. Mater. 28 (2006) 1058–1063.
[17] Z. Wu, B. Wang, Film Growth, Science Press, 2001„ p. 160 (in Chinese).
[18] L. Yao, Fundamental of Crystal Growth, University of Science and Technology of China Press, 1995,, p. 297 (in Chinese).
[19] J. Liu, Ion Beam Deposition Film Technology and Application, National Defence Industry Press, 2003,, p. 13 (in Chinese).